Self-Diffusion along Edge Dislocations in Nickel*

M. WUTTIG† AND H. K. BIRNBAUM
Department of Mining, Metallurgy and Petroleum Engineering and Materials Research Laboratory, University of Illinois, Urbana, Illinois

(Received 14 December 1965; revised manuscript received 11 February 1966)

We have measured self-diffusion along widely spaced edge dislocations in nickel. A surface-accumulation counting technique was used. The dislocations were arranged to be perpendicular to the surface which was counted and were pure edge in character. The diffusion measurements were carried out in the temperature range of 500 to 600°C where lattice diffusion was not significant. Solutions of the diffusion equation for a variety of boundary conditions are presented. The operative boundary conditions in the present experiment were determined by a tracer-sectioning technique. The diffusivity along the edge dislocations can be described by $D_p^{edge}=(20\ cm^2/sec)[\exp(-1.6\ eV/kT)]$. $Q_p^{edge}/Q_{bulk}=0.55$. The analysis of the data results in a value for the radius of the high-diffusivity dislocation core of about 10^{-7} cm.

INTRODUCTION

IT is now widely recognized that dislocation cores are regions in which enhanced diffusion can take place.[1] The most direct experimental evidence comes from diffusion experiments using bicrystals with low-angle tilt or twist boundaries.[2,3] Applying a dislocation model to these boundaries, values for the diffusivities along edge and screw dislocations were obtained. However, although the observed anisotropy of the grain boundary diffusion[4] supports the concept that grain-boundary diffusion enhancement is caused by dislocation pipe diffusion, there are two points of uncertainty remaining. First, since the spacing of the dislocations in the lowest angle grain boundaries used in the experiments referred to above (tilt and twist angles of nine and ten degrees, respectively) is of the order of six Burgers vectors, the observed grain-boundary diffusion enhancement occurred in the presence of a large amount of overlap between the stress fields of the dislocations. Secondly, the analysis of the grain-boundary-diffusion problem which has been applied requires an estimate of the width of the high-diffusivity region at the boundary. It has been generally assumed that this width is of the order of the Burgers vector. However, there is no independent support for this estimate.

The present experiment has been undertaken to examine self-diffusion along widely separated edge dislocations under conditions where the analysis is not dependent upon the estimates of the dislocation core size. Self-diffusion studies in plastically deformed nickel single crystals performed at temperatures less than half the melting temperature will be described. Several solutions of the diffusion equation which are potentially applicable to the problem will be discussed and applied to the experimental data. Values of the diffusivity of edge dislocations and of the "core diameter" will be derived. Nickel has been chosen because its isotope ^{63}Ni is ideally suited for the experimental technique used.[5]

EXPERIMENTAL PROCEDURE

Single crystals were grown from nickel of nominally 99.999% purity in an electron-beam zone-refining device. Rectangular bars about 20 mm×5 mm×3 mm in size having the orientation shown in Fig. 1(a) were cut from these crystals using a spark-erosion machine. The bars were plastically deformed by bending them around a 3-in.-diam mandril using the $[12\bar{1}]$ axis as the bending axis. The bending operation resulted in single slip on the $(\bar{1}11)$ plane in the [101] direction. Single-crystal plates having faces parallel to the $(12\bar{1})$ plane and of approximately 0.012-in. thickness were cut from these bars. The wafers were then chemically polished using a solution of 30 vol% HNO_3, 40 vol% HCl, 10 vol% H_3PO_4, and 20 vol% CH_3COOH. Sufficient material was removed by polishing to remove the surface damage introduced by the spark-cutting process. The wafers were given a 24-h anneal at 900°C in an atmosphere of 10 vol% CO, 90 vol% CO_2. (This atmosphere will reduce NiO and is in equilibrium with a carbon concentration in the Ni of

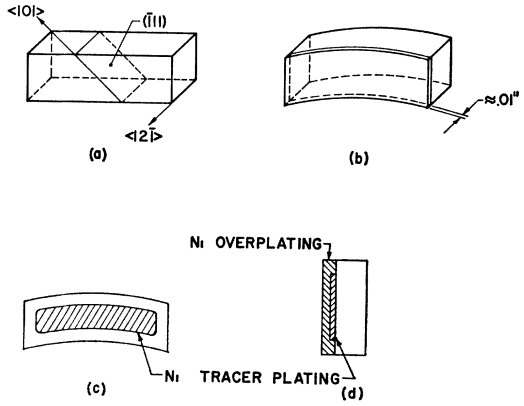

FIG. 1. Specimen orientation and configuration.

* This research was supported by the U. S. Atomic Energy Commission, Contract AT(11-1)-1198 and the National Science Foundation Contract 3208.

† On leave from Physikalisch-Technische Bundesanstalt, Institut Berlin.

[1] P. G. Shewmon, *Diffusion In Solids* (McGraw-Hill Book Company, Inc., New York, 1963).

[2] D. Turnbull and R. E. Hoffman, Acta Met. 2, 419 (1954).

[3] G. Love and P. G. Shewmon, Acta Met. 11, 899 (1963).

[4] R. E. Hoffman, Acta Met. 4, 97 (1956).

[5] A. A. Hendrickson and E. S. Machlin, Trans. AIME 6, 1035 (1954).

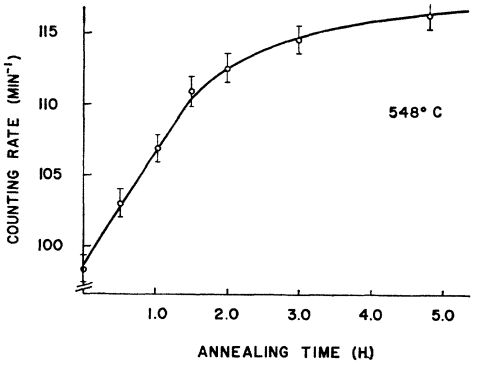

FIG. 2. Counting rate versus annealing time at 548°C.

10^{-7} atom fraction.) Back-reflection Laue photographs taken of the annealed wafers showed that the wafer orientation was preserved, no asterism was present, and indicated maximum subgrain boundary misorientation of 1.5 deg. Dislocation-etch-pit studies using an etchant consisting of 50 vol% conc. HNO_3 and 50 vol% distilled water showed that the dislocations were straight and penetrated the wafer perpendicularly to the plane of the wafer. The etch-pit pattern was identical on both faces of the wafer and through the wafer thickness indicating that the dislocations lay along the $[12\bar{1}]$. Since the slip direction was [101] the dislocations were primarily edge dislocations. The average dislocation density taken from etch-pit counts was of the order of 10^7 cm^{-2}.

A 1000-Å-thick layer of the ^{63}Ni tracer was electroplated on an area of 0.2 cm^2 on one side of the wafer using a carrier-free saturated oxalic acid solution into which the desired amount of tracer (^{63}Ni in aqueous solution as $NiCl_2$ having a specific activity 11 000 mc/g) was dissolved. (The major contaminant was ^{60}Co having a specific activity of 0.1 mc/g.) The other side of the wafer and the rim of the plated side were masked off with a lucite-benzene lacquer as indicated in Fig. 1(c). Autoradiographs confirmed the uniformity of the tracer plating. The tracer plating was covered with a protective over-plating of nonradioactive nickel that covered the whole plated side. This procedure resulted in diffusion samples as shown in Fig. 1(d).

A low-background beta counter was used to monitor the tracer flux through the wafer. It consisted of a thin-window gas-flow counter and a gamma counter. The latter was used with anticoincidence circuits to cancel cosmic radiation counts. Both counters were housed in a 5-in. lead shielding. Typical background counting rates achieved were 0.35 counts/min. The wafers could be repositioned under the counter such that the counting rates were reproduced to within 3%.

The wafers were positioned under the counter with the nonplated side facing it. The maximum energy of the beta radiation emitted from the ^{63}Ni tracer is 67 keV. Beta rays of this energy are attenuated by a factor of $1/e$ by a thickness of nickel of about 1 μ. Thus, only beta radiation emitted from tracer atoms located close to the nonplated side can be counted. The wafer thickness will totally self-shield the radiation emanating from the plated side. This self-shielding feature of the counting geometry is an essential advantage of the experimental technique and can only be accomplished if pure weak beta emitters such as ^{63}Ni are used as a tracer. The absorption of the beta radiation will produce x rays having wavelengths of the order of 0.2 Å which have a linear absorption coefficient of the order of 12 cm^{-1}. As will be shown shortly, an experimental increase of intensity of the order of $dI/I \approx 0.15$ was observed at the nonplated surface. This would correspond to a lattice penetration of the ^{63}Ni into the specimen of about 10^{-2} cm if it was caused by the x rays. As shown in the discussion this is orders of magnitude greater than can be expected from lattice diffusion under the present experimental conditions. Therefore, the observed increases of intensity cannot be due to x rays; which may however provide a part of the constant background. (The counter used has an efficiency for 67-keV x rays, which is a factor of 30 less than for 67-keV beta radiation.)

The trace impurity in the tracer, ^{60}Co, emits a 1.17-meV and a 1.33-meV photon and a 0.314-meV beta radiation. Gamma radiation of this energy will not be counted because of the anticoincidence circuitry. The range of the 0.314 beta radiation in nickel is about 9×10^{-3} cm. The experimentally observed increase in intensity, $dI/I \approx 0.15$, would correspond to a lattice diffusion of Co into the Ni specimen of about 0.9×10^{-3} cm if it was caused by the Co betas. As shown in the discussion these are orders of magnitude greater than can be expected from lattice diffusion. Therefore, the observed increases of intensity cannot be due to the ^{60}Co beta radiation; which, however, provides a part of the constant background.

The diffusion measurements were performed by measuring the activity of the wafer from the nonplated side as a function of annealing time. The temperature of the specimen was controlled to ±0.02°C and measured to ±0.5°C during the diffusion anneals which were performed in the CO-CO_2 mixture described above. The specimen was placed into a lightweight basket made of

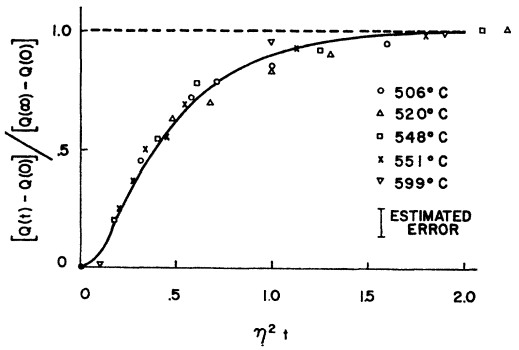

FIG. 3. Normalized activity versus reduced annealing time. (See text for the normalization procedure.)

tantalum sheet suspened on a thin wire and which could be lowered and raised by a magnetic device, operated externally. Because of the small heat capacity of the specimen assembly, the time required for the specimen temperature to be raised to the diffusion temperature and for the specimen to be gas-quenched to room temperature after each anneal was of the order of 1 min. Consequently, no corrections were applied to the annealing times used. Since the counting technique was nondestructive a single specimen was used for all the measurements of each run.

RESULTS

Figure 2 shows a typical plot of the counting rate measured from the nonplated side versus annealing time. Three features can be noted in the data: (a) The counting rate of the nonplated side increased with annealing time. As will be discussed below, this increase can only be understood if enhanced dislocation pipe diffusion occurs. (b) The rate of increase of the counting rate decreased with annealing time, indicating a saturation phenomenon which will be seen to be very important in interpreting the data. (c) The counting rate for zero annealing time is significantly higher than the background counting rate of the counting system used. This last observation was due to the 0.314-meV beta of the ^{60}Co contaminant of the tracer, to x rays which result from absorption of the ^{63}Ni beta radiation, and to back scattering of radiation from the plated side. The increase of activity with annealing time was measured in the temperature range 500–600°C and the data are shown in Fig. 3. (The specimen dimensions are listed in Table I.) As will be shown shortly the coordinates chosen in Fig. 3 reduce the data to a single curve.

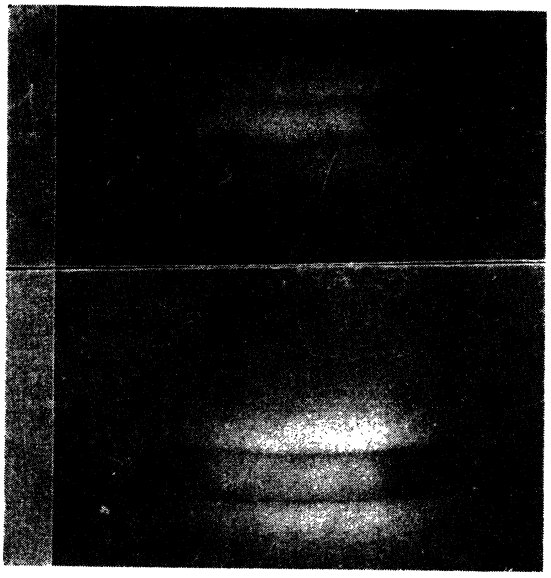

FIG. 4. Autoradiographs of nonplated wafer face before (a) and after (b) a diffusion anneal. Exposure times differ for (a) and (b).

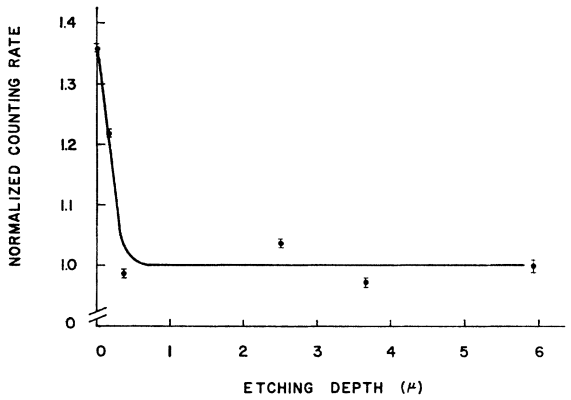

FIG. 5. Tracer counting rate versus distance from the nonplated surface after a diffusion anneal of 1000 min at 550°C.

Autoradiographs were taken of the nonplated side of all the wafers before the first and after the last diffusion anneal (Fig. 4). Microdensitometer traces taken across the radiograph obtained after the diffusion anneal showed that no additional intensity was introduced between the edge of the specimen and the central area. The darkening around the outside of the specimen was due to radiation backscattered from the plating as can be seen from the sharp outline of the specimen perimeter. The observation that the rim of the specimen was free of tracer rules out the possibility of tracer transport by surface diffusion or by vapor phase transport.

It was observed that no successful diffusion runs could be performed below 500°C. The measured increase in counting rate of the nonplated side was barely detectable at 480°C and no increase at all could be observed at lower temperatures. This point will be subsequently discussed. At temperatures above 600°C the annealing times became too short to yield reliable results.

Sectioning experiments[6] were performed on the specimens after the diffusion anneal to determine the distribution of tracer throughout the speciemn volume. The chemical etchant used was 50% HNO_3 and 50% CH_3COOH. Sections having a uniform thickness of the order of tenths of a micron could be removed. Figure 5 shows the intensity measured on the specimen face versus distance from the nonplated surface. The results

TABLE I. Summary of specimen parameters and derived experimental results.

Annealing temperature (°C)	Specimen thickness l (cm)	η^2 (sec^{-1})	k^2/η^2	$D_p=a^2$ ($cm^2\ sec^{-1}$)	r_0 (cm)
506	0.020	1.0×10^{-5}	0.1	4.0×10^{-9}	2×10^{-7}
520	0.015	2.7×10^{-5}	0.1	6.1×10^{-9}	3×10^{-7}
548	0.011	1.2×10^{-4}	0.1	1.5×10^{-8}	3×10^{-7}
551	0.015	9×10^{-5}	0.1	2.0×10^{-8}	3×10^{-7}
599	0.017	1.7×10^{-4}	≤0.3	4.9×10^{-8}	$\leq4\times10^{-7}$

[6] F. D'Alessandro, M.S. thesis, University of Illinois, 1965 (unpublished).

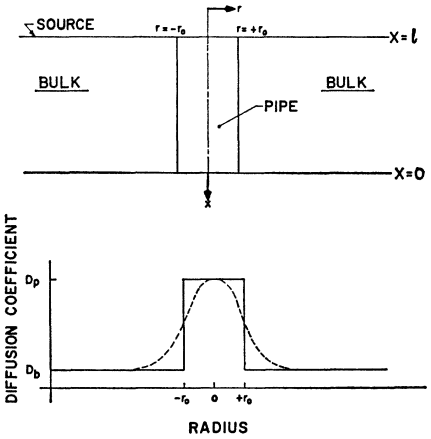

FIG. 6. Schematic of the dislocation pipe configuration and the variation of the diffusivity with radial distance from the dislocation center. Solid curve—assumed variation of diffusivity with distance. Broken curve—schematic representation of probable variation of diffusivity with distance.

of these experiments indicated that the increases in measured intensity were due to tracer material transported towards the nonplated side by diffusion and located within 0.3 μ of the nonplated side. (The activity in the second section was due largely to the difficulty in removing completely uniform sections.)

DISCUSSION

For the temperatures and times used in the present experiment, the maximum lattice "penetration depth," $2(D_b/t)^{1/2}$, is calculated to be 6×10^{-7} cm using $D_b=1.3\times\exp(-2.89\text{ eV}/kT)$ as obtained from high-temperature lattice-diffusion measurements.[7] Thus, the increase of the counting rate cannot be the result of bulk diffusion. The sectioning experiments showed that the increase in intensity at the nonplated face was due to tracer atoms located within 0.3 μ of the surface and the autoradiographic results showed that the radioactive tracer cannot have reached the nonplated side of the wafer via surface diffusion around the edges or by vapor transport. It may be concluded that the observed increase in counting rate at the nonplated side of the wafer was caused by an enhanced diffusion process through the wafer, i.e., dislocation pipe diffusion.

Quantitative analysis of the experimental results requires that the diffusion equation be solved for the present specimen configuration.[8–11] In the model used it will be assumed that the dislocation pipe configuration can be described by an array of noninteracting dislocation pipes which penetrate the waver perpendicularly. (This configuration is supported by the dislocation etch-pit results.) It is further assumed that the diffusion coefficient has a value D_p inside the pipe radius r_0 and the value of the diffusion coefficient in the bulk D_b for $r>r_0$. This configuration is shown in Fig. 6. In solving the diffusion problem, one has to allow for pipe diffusion, for loss from the pipe into the bulk, and for bulk diffusion. The diffusion equations are

$$D_p\nabla^2C_p'=\partial C_p'/\partial t;\quad r<r_0$$
$$D_b\nabla^2C_b'=\partial C_b'/\partial t;\quad r>r_0$$

$C_p'=C_p'(x,r,t)=$ concentration in the dislocation pipe. (1)

$C_b'=C_b'(x,r,t)=$ concentration in the bulk crystal.

The boundary conditions at $r=r_0$ are

$$C_p'=C_b';\quad D_p(\partial C_p'/\partial r)=D_b(\partial C_b'/\partial r). \qquad (2)$$

The solutions will depend on the boundary conditions at the "entrance," $x=l$, and the "exit," $x=0$, of the pipe and on the source function. Since these are not known *a priori*, the procedure followed will be to solve the set of Eqs. (1) for all combinations of boundary conditions and then compare the results to the experiment. The detailed mathematical analysis will be given in the appendices. In the following sections the problem will be analyzed for one choice of boundary conditions.

Consider the case where

$$\begin{aligned}&\partial C_p'/\partial x=0;\quad x=l,\\ &C_p'=0;\quad x=0,\,2l,\\ &C_p'=\alpha[\delta(x-l)+\delta(x+l)];\quad t=0,\\ &C_b'=0;\qquad\qquad\qquad t=0,\end{aligned} \qquad (3)$$

where δ is Dirac's delta function. This corresponds to a Green's function source of strength α at the pipe entrance and rapid surface diffusion at the pipe exit. The use of $C_b'=0$ at $t=0$ assumes no lattice transport from the plated surface which is in accord with the values of D_b in the temperature range of interest. The solution of Eqs. (1) with the boundary conditions of Eqs. (2) and (3) is given in Appendix A. The expressions resulting from this "exact" treatment of the diffusion problem are difficult to use in an analysis of the experiments. A somewhat simplified treatment of the problem will therefore now be presented.

Since we are interested in the diffusion along the pipe we will treat the tracer "loss" out of the pipe into the surrounding bulk as a corrective loss term. The diffusion equation for this case is derived from Fig. 6. Assuming no radial concentration gradients inside the pipe, i.e., $C_p=C_p(x,t)$, the rate of change of tracer concentration in the volume element πr_0^2dx is given by

$$\pi r_0^2dx(\partial C_p/\partial t)=[-D_p(\partial C_p/\partial x)_x+D_p(\partial C_p/\partial x)_{x+dx}]\pi r_0^2 +D_b(\partial C_b/\partial r)_{r=r_0}2\pi r_0dx. \qquad (4)$$

[7] R. E. Hoffman, F. W. Pikus, and R. A. Ward, Trans. AIME **206**, 483 (1956).

[8] A number of solutions of the problem of diffusion along isolated dislocations have been published (Refs. 9–11). The form of these solutions and the boundary conditions applied are not applicable to the present investigation.

[9] M. G. Brebrec, C.E.A. Report, DM 144, March 1965 (unpublished).

[10] Lars C. Luther, J. Chem. Phys. **43**, 2213 (1965).

[11] J. P. Stark, J. Appl. Phys. **36**, 3938 (1965).

TABLE II. Theoretical expressions for counting rates as measured from the nonplated face versus annealing time.

Case	Boundary conditions $x=l$	Boundary conditions $x=0$	$Q^*(t)$
I	$C_p=\alpha_0$	$C_p=0$	$\eta^2 t+\frac{\eta^2}{2k^2}-\frac{\eta}{2k}\coth\left(\frac{k}{\eta}\right)+2\pi^2\frac{\eta}{k}\sinh\left(\frac{k}{\eta}\right)\sum_{n=1}^{\infty}\frac{(-1)^{n-1}n^2}{\zeta_n}\exp[-\zeta_n\eta^2 t]$
II	$C_p=\alpha_0$	$\frac{\partial C_p}{\partial x}=0$	$1+k^2t-\pi\cosh\left(\frac{k}{\eta}\right)\sum_{n=1}^{\infty}\frac{(-1)^{n-1}(2n-1)}{\xi_n}\left(\exp[-\xi_n\eta^2 t]+\frac{k^2}{\eta^2\xi_n}\{1-\exp[-\xi_n\eta^2 t]\}\right)$
III	$\frac{\partial C_p}{\partial x}=\frac{\alpha\delta(t)}{a^2}$	$C_p=0$	$1-\pi\cosh\left(\frac{k}{\eta}\right)\sum_{n=1}^{\infty}\frac{(-1)^{n-1}(2n-1)}{\xi_n}\exp[-\xi_n\eta^2 t]$
IV	$\frac{\partial C_p}{\partial x}=\frac{\alpha\delta(t)}{a^2}$	$\frac{\partial C_p}{\partial x}=0$	$1-\frac{\eta}{k}\sinh\left(\frac{k}{\eta}\right)\sum_{n=1}^{\infty}(-1)^{n-1}\left[1-\frac{k^2}{\eta^2\zeta_n}\right]\exp[-\zeta_n\eta^2 t]$
			$k^2=\frac{2D_b}{r_0^2\ln(r_m/r_0)};\ \eta^2=\frac{D_p}{l^2};\ \zeta_n=n^2\pi^2+\frac{k^2}{\eta^2};\ \xi_n=\frac{(2n-1)^2\pi^2}{4}+\frac{k^2}{\eta^2}$

Expanding $(\partial C_p/\partial x)_{x+dx}$ into a Taylor series and neglecting second-order terms results in

$$D_p(\partial^2 C_p/\partial x^2)-(2/r_0)D_b(\partial C_b/\partial r)_{r=r_0}=(\partial C_p/\partial t) \quad (5)$$

for $r\leq r_0$. $(\partial C_b/\partial r)_{r=r_0}$ is the gradient of the solution of the radial diffusion equation in the bulk with the boundary conditions

$$C_b(x,r_0,t)=C_p(x,t) \quad \text{and} \quad C_b(x,r_m,t)=0,$$

where r_m is the radius where $C_b(x,r,t)=0$, i.e., $r_m\simeq\frac{1}{2}\rho^{-1/2}$ and where ρ is the dislocation density. The assumptions made in treating the boundary conditions at $r=r_0$ which lead to Eq. (5) are equivalent to those used in Fisher's analysis of grain boundary diffusion.[12] The diffusion in the bulk is not treated exactly; it is assumed that the flux in the bulk surrounding the pipe is in the radial direction only. (The problem is solved without making this assumption in Appendix A.) While this can be a rather poor approximation for a sectioning experiment it is a good approximation for the surface counting technique applied where the wafer thickness $l\gg 2(D_b t)^{1/2}$. Since the flux lost to the bulk is not counted directly, the flux at $r>r_0$ will only have to be considered in a second-order approximation; the first-order approximation being the treatment of the loss in an integral fashion leading to Eq. (5).

In order to simplify Eq. (5) even further it will be assumed that the radial gradient $(\partial C_b/\partial r)$ does not depend on time. In this case the steady-state solution for the radial diffusion in a cylinder of infinite length can be used to calculate $(\partial C_b/\partial r)_{r=r_0}$. This yields

$$\begin{gathered} a^2(\partial^2 C_p/\partial x^2)-k^2 C_p=(\partial C_p/\partial t), \\ k^2=2D_b/[r_0^2\ln(r_m/r_0)], \\ a^2=D_p. \end{gathered} \quad (6)$$

The loss from the pipe will be underestimated using the steady-state approximation of Eq. (6). For small times the $(\partial C_b'/\partial r)_{r=r_0}$ will be much larger than the steady-state value. However, as shown in Appendix D, the difference between the steady-state approximation and the exact treatment is negligible for the experimentally accessible times in the case of $D_p\gg D_b$. Solutions of Eq. (6) for various sets of boundary conditions (including the previously discussed case) and the initial condition $C_p(x,0)=0$ are given in Appendix C. Using the solutions for C_p, the intensity $Q=Q(t)$ seen by the counter from the nonplated side has been calculated in each case.

The relation between Q and C_p will depend on the boundary condition at $x=0$. For an "open pipe" and rapid surface diffusion at $x=0$, i.e., $C_p(0,t)=0$, the tracer material will be distributed over the nonplated surface. The counting rate is therefore given by

$$Q=-\nu\pi r_0^2\int_0^t D_p[\partial C_p(x,t')/\partial x]_{x=0}dt', \quad (7)$$

where ν = number of dislocation pipes operative. For a "plugged pipe" (slow surface diffusion), $(\partial C_p/\partial x)_{x=0}=0$ and the tracer material is distributed along the dislocation pipes. On defining x_0 as a cutoff depth given by the relation

$$x_0 C_p(0,t)=\int_0^\infty \exp(-\gamma x)C_p dx,$$

where γ is the absorption constant;

$$Q=\nu\pi r_0^2 x_0\left[C_p(0,t)+k^2\int_0^t C_p(0,t')dt'\right], \quad (8)$$

as shown in Appendix B.

The expressions obtained for Q in Appendix C are summarized in Table II for the various boundary conditions. The proportionality constants derived in the appendices have been omitted to facilitate a comparison of the kinetics of the various cases treated. In each case

[12] J. C. Fisher, J. Appl. Phys. 22, 74 (1951).

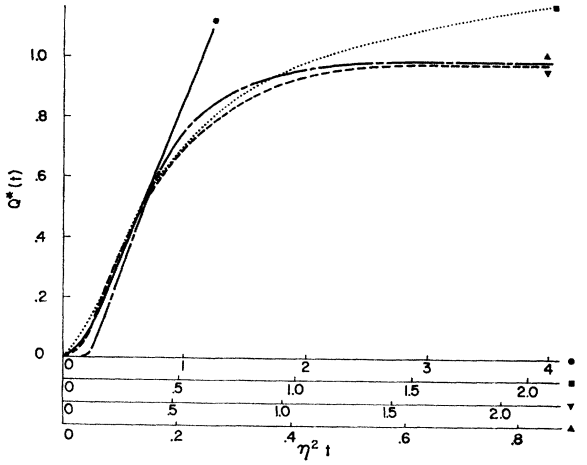

FIG. 7. Calculated curves for the tracer intensity measured on the nonplated face as a function of the reduced time, $\eta^2 t$.

- ● Case I, Appendix C.1.
- ■ Case II, Appendix C.2.
- ▲ Case III, Appendix C.3.
- ▼ Case IV, Appendix C.4.

The symbols identify the curves and the corresponding reduced times scales. The reduced time scale has been chosen so that $Q^*(t)=0.5$ at the same point for all four cases.

the correction for loss of the tracer from the pipe to the bulk is dependent on the term $(k/\eta)^2$ where $\eta^2=a^2/l^2$. (See Appendix C.) The time-dependent parts of $Q(t)$, $Q^*=Q^*(t)$, are shown in Fig. 7 for $(k/\eta)^2=0.1$. The reduced time abscissa, $t^*=\eta^2 t$, has been adjusted so that $Q^*=0.5$ at the same point in all cases.

Case I boundary conditions correspond physically to a constant source concentration (fast surface diffusion at $x=l$) and fast surface diffusion at the pipe exits ($x=0$) which distributes the tracer over the unplated surface. The total number of tracer atoms transported to the surface will be shown to be small so $C_p(0,t)=0$ for this case. These boundary conditions lead to Q which increases monotonically with time. Case II boundary conditions correspond to fast surface diffusion at the pipe entrance and slow surface diffusion at the exit so that the tracer atoms leave the pipe via diffusion through the lattice. This case results in $Q(t)$ which increases rapidly as the tracer is distributed along the pipe and then continues to increase slowly as the tracer diffuses from the pipe to the bulk. Case III corresponds to a depletable source at the dislocation entrance (which may be due to slow surface diffusion at $x=l$) and to fast surface diffusion at the dislocation exit, $x=0$. In this case the tracer atoms from the source are located primarily on the plane $x=0$ and Q increases up to an asymptotic value. Case IV corresponds to a depletable source at the pipe entrance and slow surface diffusion at $x=0$. In this case the tracer from the source is rapidly distributed along the pipe and then slowly diffuses into the lattice. Q for these conditions will show a slow increase with time to an asymptotic value but the magnitude of Q can be shown to be negligibly small.

On comparing the time dependence of Q for the four choices of boundary conditions with Fig. 3 it is readily seen that Case I does not fit the experimental data since it does not lead to the observed approach of Q to a constant value. Cases II, III, and IV cannot be distinguished on the basis of the diffusion kinetics. However, the sectioning experiments described indicated that the tracer material that had diffused through the wafer was located very close to the nonplated surface. This observation rules out Cases II and IV and is in agreement with the boundary conditions of Case III.

Figure 3 shows the normalized experimental counting rates, $[Q(t)-Q(0)]/[Q(\infty)-Q(0)]$, versus the reduced time, $t^*=\eta^2 t$. The solid curve is the calculated curve using Case-III boundary conditions. All of the data for the various temperatures can be reduced to a single curve by suitable choice of the parameters $(k/\eta)^2$ and η^2 (which depend on the values of D_p and r_0) for each temperature. The numerical values of these parameters are given in Table I. The values of D_b extrapolated from the high-temperature measurements and $r_m=3\times10^{-4}$ cm were used. The calculated curve in Fig. 3 corresponds to $(k/\eta)^2=0.1$. It is seen that the calculated curve is in excellent agreement with the experimental data.

The parameters $(k/\eta)^2$ and η^2 obtained from the curve-fitting procedure were used to calculate D_p and r_0 at each temperature (Table I). Within the accuracy of the present experiments, the temperature dependence of k^2/η^2 could not be resolved. The results for D_p are plotted in Fig. 8 versus the inverse absolute temperature. The data indicate an activation energy of self-diffusion along edge dislocation pipes of 1.6 eV and a pre-exponential factor of 20 cm^2 sec^{-1}. The expression

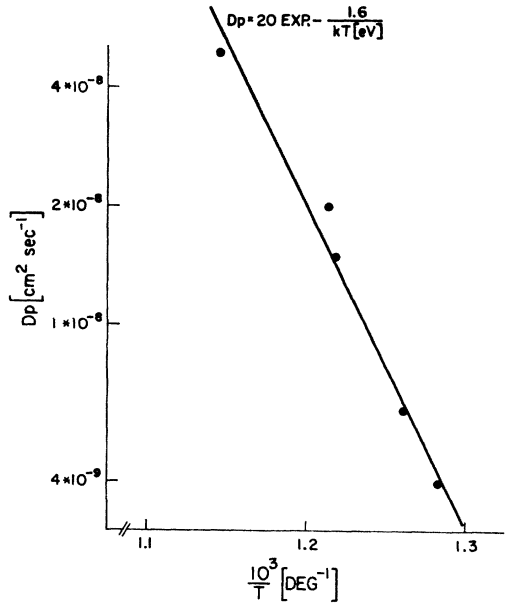

FIG. 8. Arrhenius plot of the measured edge dislocation diffusivities.

for diffusion along edge dislocations:

$$D_p(\text{edge}) = 20 \text{ cm}^2 \text{ sec}^{-1} \exp(-1.6 \text{ eV}/kT)$$

should be compared to that for bulk diffusion[7]:

$$D_b = 1.3 \text{ cm}^2 \text{ sec}^{-1} \exp(-2.89 \text{ eV}/kT).$$

It is observed therefore that

$$Q_p/Q_b(\text{edge}) = 0.55.$$

The amount of radioactive tracer material plated onto the wafer should result in a constant concentration at the pipe entrance if surface diffusion were fast at $x=l$. However, the experiments indicate an exhaustible source which means that only a limited amount of tracer is actually funneled into the dislocation pipes. The boundary conditions at the dislocation pipe entrance depend on the diffusion process occurring at specimen-plate interface which will depend on the structure of the plate at the dislocation entrance. The observation that no intensity increase could be obtained below 490°C suggests that tracer is supplied by bulk diffusion. $2(D_b t)^{1/2}$ becomes comparable to the lattice parameter of nickel for the longest annealing times used at 490°C. At the temperatures for which successful diffusion runs are reported it is concluded that the dislocation pipe drains tracer only from a very small volume at its "entrance."

A consideration of the total increase of the counting rate from the nonplated side leads to the same conclusion. The volume V from which the dislocation pipe drains is given by

$$V = [Q(\infty) - Q(0)]/(22.2 \times 10^{11} \alpha \rho \nu \gamma), \quad (9)$$

$Q(\infty) - Q(0)$ = total increase in counting rate [counts min^{-1}],

α = fraction of 4π covered by the counting assembly; $\alpha = 0.1$,

ρ = specific weight of nickel,

γ = specific activity of ^{63}Ni in Curies gram^{-1}.

Assuming a spherical volume, the values for the present experiment yield $r \simeq 2 \times 10^{-7}$ cm. This shows again that the pipes are draining tracer atoms from a very small volume. For the observed increases in counting rates, the maximum tracer concentration at $x=0$ is $C_p(0,t) \sim 10^{-6}$ which supports the assumption that the sink capacity of the nonplated side is infinite.

At the present time the details of the diffusion processes at $x=0$, l which correspond to the observed boundary conditions are not fully understood. The difference in the boundary conditions may result from the fact that $x=l$ corresponds to the interface between the crystal and the plate while $x=0$ corresponds to a crystal surface.

The mean value of the dislocation pipe radius is $r_0 \approx 2 \times 10^{-7}$ cm or $r_0 \sim 6$ Burgers vectors. The treatment of the data outlined above does not depend on the value of the dislocation density except through the parameter r_m and is insensitive to the value of r_m. However, since r_0 is obtained from consideration of the radial loss correction to the flux along the dislocation and depends on the value of D_b extrapolated from elevated temperatures, the precision with which it is known is not high. As shown schematically in Fig. 6, r_0 is defined as the radius at which the diffusivity decreases to the mean value between the value at the dislocation center and that of the bulk. While the correspondence between the dislocation core defined in this fashion and the radius at which the strains due to the dislocation become large is not established the two "core radii" are about equal. The value of r_0 is also consistent with the partial dislocation separation calculated using a stacking fault energy of 150 ergs/cm^2. (The effect of partial dislocation separation on r_0 is presently being investigated.)

The two main results of the experiment described are the activation energy of self-diffusion along edge dislocations in nickel and an estimate for the core radius. Both numbers characterize properties of the dislocation core about which little is known as yet. Thus, only some very qualitative remarks can be made. Self-diffusion along high-angle tilt boundaries has been studied in nickel by Upthegrove and Sinnott[13] who obtained $Q_{\text{boundary}} = 1.13$ eV ($Q_{\text{boundary}}/Q_b = 0.39$). Wazzan[14] obtained $Q_{\text{boundary}} = 1.19$ eV ($Q_{\text{boundary}}/Q_b = 0.41$) for diffusion along random high-angle boundaries in nickel. Q_{boundary}/Q_b for high-angle tilt[2] and twist[3] boundaries in silver is 0.44 and 0.40, respectively. The value of $Q_p/Q_b = 0.55$ obtained for isolated edge dislocations in nickel is somewhat larger than the values obtained for Q_{boundary}/Q_b. Since the structure of the high-angle boundaries used in the above investigations is probably more complex than assumed in interpreting the grain boundary diffusion data the differences are not unexpected.

If a vacancy diffusion mechanism is operative at the edge dislocations, $Q_p = E_f' + E_m'$ where E_f' is the vacancy formation energy and E_m' is the vacancy motion energy at the dislocation. At the present time it is not possible to separate Q_p into E_f' and E_m'. However, since $E_f' + E_m' = 0.55\,(E_f + E_m)$ where E_f and E_m are the vacancy formation and motion energies in the lattice we can write

$$E_m' \approx 0.55 E_m - 0.45 E_f + B,$$

where B is the binding energy of the vacancy to the dislocation. Studies[15] of the annealing of quenched-in resistivity in nickel lead to the value $E_m = 1.0$ eV. Since $Q_b = E_f + E_m = 2.89$ eV,

$$E_m' \approx (B - 0.3) \text{ eV}, \quad \text{and} \quad E_f' \approx (1.89 - B) \text{ eV}.$$

[13] W. R. Upthegrove and M. J. Sinnott, Trans. Am. Soc. Metals **50**, 1031 (1958).

[14] Ahmed Rassem Wazzan, J. Appl. Phys. **36**, 3596 (1965).

[15] M. Wuttig and H. K. Birnbaum, J. Phys. Chem. Solids **27**, 225 (1966).

Therefore, 0.3 eV$\leq B\leq$1.89 eV. Calculations[16] indicate $B\approx$0.4 eV. This value leads to the result $E_m'\ll E_f'$.

ACKNOWLEDGMENTS

The authors would like to express their sincere appreciation for the assistance of Frank D'Alessandro who very ably carried out the sectioning experiments. They would also like to thank Dr. D. Lazarus for helpful discussions and for the use of the counting facility.

APPENDIX A: CALCULATION OF THE FLUX ONTO THE NONPLATED SIDE USING EQS. (1)

For radial symmetry Eqs. (1) are written

$$D_p\left(\frac{\partial^2 C_p'}{\partial r^2}+\frac{1}{r}\frac{\partial C_p'}{\partial r}+\frac{\partial^2 C_p'}{\partial x^2}\right)=\frac{\partial C_p'}{\partial t},\quad r<r_0,$$

$$D_b\left(\frac{\partial^2 C_b'}{\partial r^2}+\frac{1}{r}\frac{\partial C_b'}{\partial r}+\frac{\partial^2 C_b'}{\partial x^2}\right)=\frac{\partial C_b'}{\partial t},\quad r>r_0, \tag{A1}$$

$$C_p'=C_p'(x,r,t),\qquad C_b'=C_b'(x,r,t).$$

This set of equations can be solved for the boundary conditions of Eqs. (2) and (3). On applying the finite Fourier-Laplace transformation

$$\hat{C}_p'=\int_0^{2l}\int_0^{\infty} C_p'\sin(n\pi x/2l)\exp(-pt)dtdx,$$

$$\hat{C}_b'=\int_0^{2l}\int_0^{\infty} C_b'\sin(n\pi x/2l)\exp(-pt)dtdx,$$

one obtains

$$\frac{\partial^2\hat{C}_p'}{\partial r^2}+\frac{1}{r}\frac{\partial\hat{C}_p'}{\partial r}-k_{pn}^2\hat{C}_p'+\frac{2\alpha}{D_p}\sin\left(\frac{n\pi}{2}\right)=0,\quad r<r_0$$

$$\frac{\partial^2\hat{C}_b'}{\partial r^2}+\frac{1}{r}\frac{\partial\hat{C}_b'}{\partial r}-k_{bn}^2\hat{C}_b'=0,\quad r>r_0 \tag{A2}$$

where

$$k_{pn}^2=(n\pi/2l)^2+p/D_p,\quad k_{bn}^2=(n\pi/2l)^2+p/D_b.$$

The solutions of Eqs. (A2) which obey the transformed boundary conditions and remain bounded for $0\leq r\leq\infty$ are

$$\hat{C}_p'=\frac{2\alpha\sin(n\pi/2)}{D_pk_{pn}^2}\left[1-\frac{D_bk_{bn}K_1(k_{bn}r_0)}{\rho'}I_0(k_{pn}r)\right],$$

$$\hat{C}_b'=\frac{2\alpha\sin(n\pi/2)}{D_pk_{pn}^2}\left[\frac{D_pk_{pn}I_1(k_{pn}r_0)}{\rho'}K_0(k_{bn}r)\right], \tag{A3}$$

where

$$\rho'=D_pk_{pn}I_1(k_{pn}r_0)K_0(k_{bn}r_0)+D_bk_{bn}I_0(k_{pn}r_0)K_1(k_{bn}r_0).$$

The Laplace transform of the intensity on the nonplated surface is given by an equation equivalent to Eq. (7)

$$\bar{Q}'(p)=-\nu D_p\int_0^t\int_0^{2\pi}\int_0^{r_0}(\partial\bar{C}_p'/\partial x)_{x=0}rdrd\Phi dt, \tag{A4}$$

where $\bar{C}_p'=\bar{C}_p'(x,r,p)$ is obtained from the inverse Fourier transform of $\hat{C}_p'$. Using the integral theorem for the Laplace transform and the identity

$$\sum_{n=1}^{\infty}\frac{n\sin(n\pi/2)}{y^2+n^2}=-\frac{\pi/2}{\cosh(y\pi/2)}.$$

$\bar{Q}'(p)$ is given by

$$\bar{Q}'(p)=\frac{\nu\pi\alpha r_0^2}{p\cosh[l(p/D_p)^{1/2}]}-\nu D_b\frac{\pi\alpha r_0^2}{l^2}\sum_{n=0}^{\infty}\bar{q}(n,p)\sin(n\pi/2), \tag{A5}$$

where

$$\bar{q}(n,p)=\frac{K_1(k_{bn}r_0)I_1(k_{pn}r_0)}{pk_{pn}^3\rho'}.$$

The inverse of $\bar{q}$ is a sum of three contributions

$$q=q_1+q_2+q_3.$$

The contribution from the pole $p=0$ is

$$q_1=\frac{K_1(\beta_nr_0)I_1(\beta_nr_0)}{r_0^4\beta_n^4[D_pI_1(\beta_nr_0)K_0(\beta_nr_0)+D_bI_0(\beta_nr_0)K_1(\beta_nr_0)]},$$

$$\beta_n=n\pi/2l. \tag{A6}$$

The contribution from the branch point at $p=-\beta_n^2D_p$ is obtained by making the substitutions $\epsilon\exp(i\theta)=Z$ and using the partial fraction expansion for $I_\nu(Z)/I_{\nu-1}(Z)$.[17]

$$q_2=[\exp(-\beta_n^2D_pt)]/\beta_n^2D_br_0^2. \tag{A7}$$

The third contribution which results from the integral along the negative real axis is

$$q_3=\frac{1}{\pi}\exp(-\beta_n^2D_bt)\int_{r_0^2\beta_n^2(\Delta-1)/\Delta}^{\infty}\exp(-D_b\mu^2t/r_0^2)\times\frac{J_1(f_n^{1/2})[\psi Y_1(\mu)-\Phi J_1(\mu)]}{D_b(\mu^2+\beta_n^2r_0^2)f_n^{3/2}(\psi^2+\Phi^2)}d\mu, \tag{A8}$$

[16] J. Friedel, *Dislocations* (Pergamon Press, Ltd., Oxford, 1964), p. 364.

[17] G. N. Watson, *Theory of Bessel Functions* (Cambridge University Press, London, 1944), Chap. 5.

where

$$f_n=\Delta\mu^2+(\Delta-1)\beta_n{}^2r_0{}^2,$$
$$\Delta=D_p/D_b,$$
$$\Phi=D_pf_n{}^{1/2}J_0(\mu)J_1(f_n{}^{1/2})+D_b\mu J_1(\mu)J_0(f_n{}^{1/2}),$$
$$\psi=D_pf_n{}^{1/2}Y_0(\mu)J_1(f_n{}^{1/2})+D_b\mu Y_1(\mu)J_0(f_n{}^{1/2}).$$

It is seen that the first term in $\bar{Q}'(p)$, Eq. (A5) is equal to the solution of the equivalent pipe diffusion problem without radial loss and retransforms as shown in Appendix C.3.

APPENDIX B: DERIVATION OF THE FORMULA

$$Q_{\text{exit}}(t)=\nu\pi r_0{}^2x_0\left\{C_p(0,t)+k^2\int_0^t C_p(0,t')dt'\right\}.$$

This relation is valid only in the cases where $(\partial C_p/\partial x)_{x=0}=0$, i.e., there is no flux from the dislocation pipe to the exit surface $x=0$. In this case the tracer counting rate can be divided into two parts: one due to the tracer located in the pipe, and the other to the tracer located in the adjacent lattice.

$$Q_{\text{exit}}(t)=Q_{\text{pipe}}+Q_{\text{lattice}}. \tag{B1}$$

Using the definition of x_0 we obtain

$$Q_{\text{pipe}}=\nu\pi r_0{}^2x_0C_p(0,t). \tag{B2}$$

In the same fashion Q_{lattice} is given by

$$Q_{\text{lattice}}=2\pi r_0x_0\nu\int_0^t D_b(\partial C_b/\partial r)_{r=r_0}dt'. \tag{B3}$$

Using the steady-state approximation for the loss flux out of the pipe into the lattice $(\partial C_b/\partial r)_{r=r_0}$ is given by

$$[\partial C_b/\partial r]_{r=r_0}=C_p/[r_0\ln(r_m/r_0)].$$

Consequently, it follows that

$$Q_{\text{lattice}}=2\pi r_0x_0\nu\int_0^t D_bC_p(0,t')/[r_0\ln(r_m/r_0)]dt'. \tag{B4}$$

Since by definition

$$k^2=2D_b/[r_0{}^2\ln(r_m/r_0)],$$

it follows that

$$Q_{\text{exit}}(t)=\nu\pi r_0{}^2x_0\left[C_p(0,t)+k^2\int_0^t C_p(0,t')dt'\right]. \tag{B5}$$

APPENDIX C: SOLUTION OF EQ. (6) FOR VARIOUS BOUNDARY CONDITIONS

C.1. The case $C_p(l,t)=\alpha_0$, $C_p(0,t)=0$, $C_p(x,0)=0$. The Laplace transform of Eq. (6) is

$$a^2(\partial^2\bar{C}_p/\partial x^2)-(k^2+p)\bar{C}_p=0,\quad a^2=D_p,$$
$$\bar{C}_p=\bar{C}_p(x,p)=\int_0^\infty \exp(-pt)C_pdt. \tag{C1}$$

The boundary conditions transform into $\bar{C}_p(l,p)=\alpha_0/p$, $\bar{C}_p(0,p)=0$. This system has the solution

$$\bar{C}_p=\alpha_0\frac{\sinh[x(k^2+p)^{1/2}/a]}{p\sinh[l(k^2+p)^{1/2}/a]}. \tag{C2}$$

Proceeding as in Appendix A we obtain for the Laplace transform of the intensity on the nonplated surface

$$\bar{Q}(p)=\nu\frac{\alpha_0\pi r_0{}^2}{a}\frac{(k^2+p)^{1/2}}{p^2\sinh[l(k^2+p)^{1/2}/a]}. \tag{C3}$$

On applying the inversion theorem

$$Q(t)=\nu\alpha_0\pi r_0{}^2l\frac{k/\eta}{\sinh(k/\eta)}\left[\eta^2t+\frac{\eta^2}{2k^2}-\frac{\eta}{2k}\coth(k/\eta)\right.$$
$$\left.+2\pi^2\frac{\eta}{k}\sinh\left(\frac{k}{\eta}\right)\sum_{n=1}^{\infty}\frac{(-1)^{n-1}n^2}{\zeta_n}\exp(-\zeta_n\eta^2t)\right], \tag{C4}$$

where

$$\eta^2=a^2/l^2,\quad \zeta_n=n^2\pi^2+k^2/\eta^2.$$

C.2. The case $C_p(l,t)=\alpha_0$, $(\partial C_p/\partial x)_{x=0}=0$, $C_p(x,0)=0$. The solution of Eq. (C1) for

$$\bar{C}_p(l,p)=\alpha_0/p,\quad (\partial\bar{C}_p/\partial x)_{x=0}=0$$

is

$$\bar{C}_p=\alpha_0\frac{\cosh[x(k^2+p)^{1/2}/a]}{p\cosh[l(k^2+p)^{1/2}/a]}. \tag{C5}$$

$\bar{Q}(p)$ is in this case obtained from Eq. (8).

$$\bar{Q}(p)=\frac{\alpha_0\pi r_0{}^2x_0\nu}{p\cosh[l(k^2+p)^{1/2}/a]}(1+k^2/p). \tag{C6}$$

The retransform is

$$Q(t)=\frac{\alpha_0\pi r_0{}^2x_0\nu}{\cosh(k/\eta)}$$
$$\times\left(1+k^2t-\pi\cosh(k/\eta)\sum_{n=1}^{\infty}\frac{(-1)^{n-1}(2n-1)}{\xi_n}\right.$$
$$\left.\times\left\{\exp(-\xi_n\eta^2t)+\frac{k^2}{\eta^2\xi_n}[1-\exp(-\xi_n\eta^2t)]\right\}\right), \tag{C7}$$

where $\xi_n=[(2n-1)\pi/2]^2+(k/\eta)^2$.

C.3. The case $(\partial C_p/\partial x)_{x=l}=\alpha\delta(t)/a^2$, $C_p(0,t)=0$, $C_p(x,0)=0$.

These boundary conditions correspond to an instantaneous source of strength α at $x=l$ and $t=0$ and are equivalent to the Green's function formalism as treated in Carslaw and Jaeger.[18] At $x=l$ an amount of tracer α

[18] H. S. Carslaw and J. C. Jaeger, *Conduction of Heat in Solids* (Oxford University Press, London, 1959), 2nd ed., Chap. 14.

enters the dislocation pipe at $t=0$, i.e.,

$$\lim_{t\to 0}\int_0^t D_p[\partial C_p(x,t')/\partial x]_{x=l}dt'=\alpha. \quad \text{(C8)}$$

Equation (C8) is satisfied if

$$(\partial C_p/\partial x)_{x=l}=\alpha\delta(t)/a^2.$$

For $t>0$, $(\partial C_p/\partial x)_{x=l}=0$ as required by the conditions of an instantaneous source.

The boundary conditions transform into $(\partial \bar{C}_p/\partial x)_{x=l}=\alpha/a^2$, $\bar{C}_p(0,p)=0$. The solution of Eq. (C1) fulfilling these boundary conditions is

$$\bar{C}_p=\frac{\alpha}{a}\frac{\sinh[x(k^2+p)^{1/2}/a]}{(k^2+p)^{1/2}\cosh[l(k^2+p)^{1/2}/a]}.$$

Retransformation yields

$$C_p=\frac{2}{l}\alpha\sum_{n=1}^{\infty}(-1)^{n-1}\exp\left\{\left[-\frac{(2n-1)^2\pi^2}{4}+\frac{k^2}{\eta^2}\right]\eta^2 t\right\}\times\sin\left[\frac{(2n-1)\pi x}{2l}\right]. \quad \text{(C9)}$$

Proceeding as in Appendix A we obtain for $\bar{Q}(p)$

$$\bar{Q}(p)=\frac{\alpha\pi r_0^2\nu}{p\cosh[l(k^2+p)^{1/2}/a]}, \quad \text{(C10)}$$

which on retransforming yields

$$Q(t)=\frac{\alpha\pi r_0^2\nu}{\cosh(k/\eta)}\left[1-\pi\cosh(k/\eta)\times\sum_{n=1}^{\infty}\frac{(-1)^{n-1}(2n-1)}{\xi_n}\exp(-\xi_n\eta^2 t)\right]. \quad \text{(C11)}$$

C.4. The case $(\partial C_p/\partial x)_{x=l}=\alpha\delta(t)/a^2$, $(\partial C_p/\partial x)_{x=0}=0$, $C_p(x,0)=0$.

The solution of Eq. (C1) for $(\partial \bar{C}_p/\partial x)_{x=l}=\alpha/a^2$, $(\partial \bar{C}_p/\partial x)_{x=0}=0$, is

$$\bar{C}_p=\frac{\alpha}{a}\frac{\cosh[x(k^2+p)^{1/2}/a]}{(k^2+p)^{1/2}\sinh[l(k^2+p)^{1/2}/a]}. \quad \text{(C12)}$$

$\bar{Q}(p)$ is in this case given by Eq. (8)

$$\bar{Q}(p)=\frac{\alpha\pi r_0^2 x_0\nu}{a(k^2+p)^{1/2}\sinh[l(k^2+p)^{1/2}/a]}(1+k^2/p). \quad \text{(C13)}$$

The inverse is

$$Q(t)=\frac{\alpha\pi r_0^2 x_0 k\nu}{a\sinh(k/\eta)}\{1-2(\eta/k)\sinh(k/\eta)\times\sum_{n=1}^{\infty}(-1)^{n-1}[1-k^2/\zeta_n\eta^2]\exp(-\zeta_n\eta^2 t)\}. \quad \text{(C14)}$$

APPENDIX D: COMPARISON OF THE SOLUTIONS OF EQS. (5) AND (6)

The radial flux out of a cylinder of radius r_0 having infinite length into an infinite medium is given by[18]

$$F(t)=C_p\frac{4D_b}{r_0\pi^2}\int_0^{\infty}\frac{\exp(-D_b\mu^2 t)d\mu}{\mu[J_0^2(r_0\mu)+Y_0^2(r_0\mu)]}, \quad \text{(D1)}$$

which on inserting into Eq. (5) yields

$$a^2(\partial^2 C_p/\partial x^2)-k'^2 C_p f(t)=\partial C_p/\partial t, \quad \text{(D2)}$$

where

$$a^2=D_p,\quad k'^2=8D_b/r_0^2\pi^2,$$

$$f(t)=\int_0^{\infty}\frac{\exp(-D_b\mu^2 t)d\mu}{\mu[J_0^2(r_0\mu)+Y_0^2(r_0\mu)]}.$$

The solution of Eq. (D2) for the conditions $(\partial C_p/\partial x)_{x=l}=\alpha\delta(t)/a^2$, $C_p(0,t)=0$, $C_p(x,0)=0$ is

$$C_p=\frac{2\alpha}{l}\sum_{n=1}^{\infty}(-1)^{n-1}\exp\left[-\frac{(2n-1)^2\pi^2 a^2}{4l^2}t-k'^2\int_0^t f(t')dt'\right]\times\cos((2n-1)\pi x/2l). \quad \text{(D3)}$$

On comparing Eqs. (D3) and (C9) it is seen that $k^2 t$ has been replaced by $L=k'^2\int_0^t f(t')dt'$. L can be rewritten as

$$L=k^2 t L_{\text{corr}} \quad \text{where} \quad L_{\text{corr}}=(k'^2/k^2 t)\int_0^t f(t')dt'.$$

Computer calculations show that L_{corr} varies within the time range where data were taken by not more than 300%, which corresponds to a change in $(k/\eta)^2$ by a factor of 3. Figure 9 shows two plots of $Q^*(t)$ for

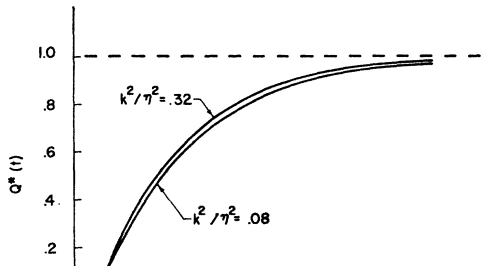

FIG. 9. Dependence of calculated Q^* versus reduced time curves on the loss parameter k^2/η^2 for Case III boundary conditions.

Case III (see Table II) for $(k/\eta)^2=3.2\times10^{-1}$ and $(k/\eta)^2=8\times10^{-2}$. On comparing the small difference between the two curves with the scatter of the data points in Fig. 3 it is seen that this difference could not be resolved. Consequently, L_{corr} can be treated as a constant independent of time which is the approximation used.

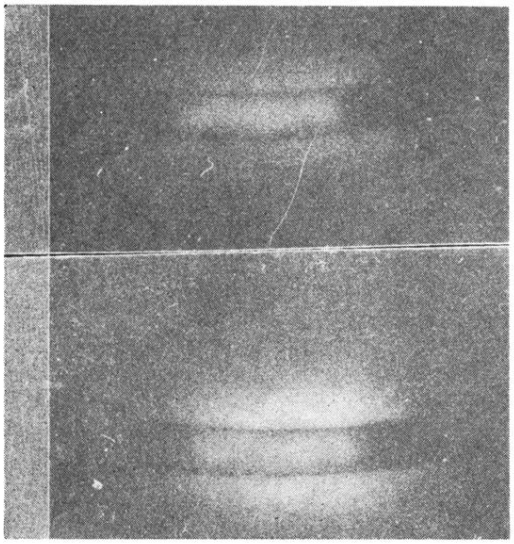

FIG. 4. Autoradiographs of nonplated wafer face before (a) and after (b) a diffusion anneal. Exposure times differ for (a) and (b).